Integrated Path Following and Collision Avoidance Using a Composite Vector Field

Yao, Weijia; Lin, Bohuan; Cao, Ming

IMPORTANT NOTE: You are advised to consult the publisher's version (publisher's PDF) if you wish to cite from it. Please check the document version below.

Document Version
Final author's version (accepted by publisher, after peer review)

Publication date:
2020

[Link to publication in University of Groningen/UMCG research database](#)

Citation for published version (APA):
Yao, W., Lin, B., & Cao, M. (2020). Integrated Path Following and Collision Avoidance Using a Composite Vector Field. In *Proceedings of the 58th IEEE Conference on Decision and Control* (pp. 250-255). IEEE. https://doi.org/10.1109/CDC40024.2019.9029903

is presented in [10]. To avoid obstacles on the path, the authors propose a method to deform the desired path slightly. However, the theoretical analysis of this method is limited in the literature. Another possible method to enable the robot to deviate from the desired path is to modify the vector field locally. This idea is reported in [11] recently. Since the combination of one vector field for path following and the other for collision avoidance may generate undesirable effects, different decay functions have been evaluated to mitigate them [11]; however, there is no theoretical guarantee for either collision avoidance or path following.

To the best of our knowledge, there are only a few papers investigating the problem of path following and collision avoidance in a unified framework. In [12], the authors design a combined path following and obstacle avoidance control law using the Deformable Virtual Zone (DVZ) method and a Lyapunov backstepping design. An inherent limitation is that the path following controller and the collision avoidance controller generate antagonistic system reactions. The authors provide a solution exploiting heuristic switching, but there is no mathematical analysis, and convergence to the path is not guaranteed. In addition, the path following functionality is achieved by controlling the rate of progression of a virtual target on the path explicitly; thus, it inherits the performance limitation of trajectory tracking algorithms. Another work [13] employs the idea of the force field and path deformation to achieve path following and collision avoidance at the same time. This approach requires low computational load; however, they only consider straight lines as the desired paths between adjacent waypoints, which may lead to large path-following error. The study [14] proposes a switching guidance system with a path following mode and a collision avoidance mode for an unmanned surface vessel (USV). Since the system relies on calculating the cross-track error, it is probably challenging to deal with paths and obstacles with shapes other than straight lines or circles. In addition, Zeno behaviour might exist in the switching system [15, Section 1.2.2].

In this paper, we propose a general and unified framework using a composite vector field to achieve collision avoidance and path following simultaneously. Rigorous theoretical analysis is provided, and thus, the behaviours of collision avoidance and path following are provably enabled. Two vector fields, one for path following and the other for collision avoidance, are generated. Inspired by "partition of unity" from topology [16, Theorem 2.23], we use bump functions, which are smooth functions that admit non-zero values on compact domains, to smoothly combine these two

Integrated Path Following and Collision Avoidance Using a Composite Vector Field

Weijia Yao, Bohuan Lin, Ming Cao

Abstract— Path following and collision avoidance are two important functionalities for mobile robots, but there are only a few approaches dealing with both. In this paper, we propose an integrated path following and collision avoidance method using a composite vector field. The vector field for path following is integrated with that for collision avoidance via bump functions, which reduce significantly the overlapping effect. Our method is general and flexible since the desired path and the contours of the obstacles, which are described by the zero-level sets of sufficiently smooth functions, are only required to be homeomorphic to a circle or the real line, and the derivation of the vector field does not involve specific geometric constraints. In addition, the collision avoidance behaviour is reactive; thus, real-time performance is possible. We show analytically the collision avoidance and path following capabilities, and use numerical simulations to illustrate the effectiveness of the theory.

I. Introduction

Path following serves as one of the most fundamental capabilities for mobile robots. Treating the desired path as a geometric object instead of a function of time, path following algorithms are able to overcome the inherent performance limitations of trajectory tracking algorithms [1]. Among different path following algorithms, the one using a vector field is shown to achieve high path-following accuracy while requiring low control efforts [2]. The principal idea behind this method is that the vector field's integral curves converge to the desired path, and thus the vector field can be used as a guidance signal for a robot [3]–[5]. Another fundamental capability of mobile robots is collision avoidance. There are already many different collision avoidance methods, such as the Artificial Potential Fields (APF) method [6], [7], the Dynamic Window (DW) approach [8] and the Vector Field Histogram (VFH) [9]. In the APF method, the goal position creates attractive force and the obstacles create repulsive force such that the combined force guides the robot to approach the goal while avoiding obstacles on the way. This method is similar to the vector-field-based path following method in the sense that they induce some kinds of vector fields to fulfil their tasks.

It is important to integrate path following with collision avoidance since during the path following process, there might be unexpected obstacles. For the sake of safety, the robot needs to compromise the accuracy of path following and deviate from the path. Recently, an experimental study

vector fields, while greatly reducing the undesirable effects of overlapping. This also guarantees the existence and uniqueness of solutions of the corresponding differential equation. Since no switching mechanism is introduced, Zeno behaviour is irrelevant. One of the advantages of our framework is its generality and flexibility. For example, since the construction of the composite vector field does not involve any specific geometric relations or constraints, the vector field is not restricted to any fixed cases. In fact, there are no particular constraints on the shapes of the desired path and the contours of obstacles as long as they are homeomorphic to a circle or the real line. Therefore, our method is even applicable in an environment with obstacles of a concave geometric shape. Another advantage is that the collision avoidance approach is reactive, implying that no motion planning or construction of symbolic maps of the environment is required. Therefore, a robot is able to locally and smoothly modify the composite vector field via bump functions when it encounters new obstacles during its movement. This enables the capability of real-time collision avoidance and path following. Note that our method is fundamentally different from the APF method in the sense that the composite vector field is not deduced from a potential function, and we do not aspire to have a unique global minimum. In fact, the control objective of following a path requires a continuous motion of the robot (e.g., an unmanned aerial vehicle) rather than just reaching the desired destination point. In addition, our method enables robots to smoothly go through narrow passages formed by closely positioned obstacles, which can hardly be achieved by the traditional APF [17].

The remainder of this paper is organized as follows. Section II presents the problem formulation. Then the design of the composite vector field is given in Section III. In Section IV, the main theoretical results are elaborated. Then some illustrative simulation examples are carried out to validate the theoretical results in Section V. Finally, Section VI concludes the paper and indicates future work.

II. PROBLEM FORMULATION

Generally speaking, we aim to obtain a control algorithm for a robot to follow a predefined desired path, and at the same time, avoid any obstacles near the path. The more precise problem setting is formulated below.

A. Desired Path

The desired path $\mathcal{P} \subset \mathbb{R}^2$ is described by the zero-level set of a twice continuously differentiable function $\phi : \mathbb{R}^2 \to \mathbb{R}$ as follows:

$$\mathcal{P} = \{\xi \in \mathbb{R}^2 : \phi(\xi) = 0\}. \tag{1}$$

It is natural to assume that $\mathcal{P}$ is a one-dimensional connected submanifold in $\mathbb{R}^2$. Thus, $\mathcal{P}$ is homeomorphic to a circle if it is compact, and the real line $\mathbb{R}$ otherwise [18, Theorem 5.27]. One of the advantages of using the zero-level set is that this facilitates the use of the value $\phi(\xi)$ at a point $\xi \in \mathbb{R}^2$ to
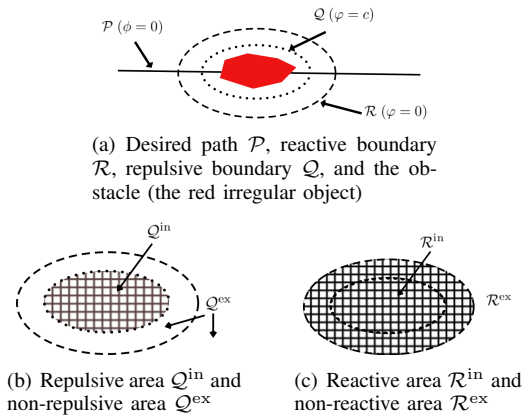

(a) Desired path $\mathcal{P}$, reactive boundary $\mathcal{R}$, repulsive boundary $\mathcal{Q}$, and the obstacle (the red irregular object)

(b) Repulsive area $\mathcal{Q}^{\mathrm{in}}$ and non-repulsive area $\mathcal{Q}^{\mathrm{ex}}$

(c) Reactive area $\mathcal{R}^{\mathrm{in}}$ and non-reactive area $\mathcal{R}^{\mathrm{ex}}$

Fig. 1. Illustrations of concepts.

"measure" the distance $\mathrm{dist}(\xi, \mathcal{P})$[1] between the point ξ and the path $\mathcal{P}$. For example, a circular path $\mathcal{P}$ can be described by using $\phi(x, y) = x^2 + y^2 - R^2$, where R is the radius of the circle. The distance function is $\mathrm{dist}(\xi, \mathcal{P}) = |\sqrt{x^2 + y^2} - R|$. Note that for every point ξ on the circle, $\mathrm{dist}(\xi, \mathcal{P}) = 0$ and $\phi(\xi) = 0$. As the value $|\phi(\xi)|$ increases, the distance between the point and the circle also increases. One easily observes that it is simpler to evaluate the distance using the $\phi(\xi)$ value rather than the distance function. This advantage is more obvious for more complicated paths, such as an ellipse. Thus we make the following assumption:

Assumption 1: For any $\xi_1, \xi_2 \in \mathbb{R}^2$, if $|\phi(\xi_1)| \leq |\phi(\xi_2)|$, then $\mathrm{dist}(\xi_1, \mathcal{P}) \leq \mathrm{dist}(\xi_2, \mathcal{P})$.

Remark 1: One may notice that this assumption is not satisfied for an ellipse if the Euclidean metric is used in the distance function $\mathrm{dist}(\cdot, \mathcal{P})$. However, this can be easily generalized by using an equivalent metric such that the convergence properties still hold (e.g., such an equivalent metric exists for an ellipse).

B. Obstacles, Reactive Areas and Repulsive Areas

Suppose there is a finite set of stationary obstacles $\mathcal{O}_{\mathrm{all}} = \{\mathcal{O}_i \subset \mathbb{R}^2 : i \in \mathcal{I}\}$, where $\mathcal{I} = \{1, 2, \ldots, m\}$ and m is the total number of obstacles. The geometric shapes of the obstacles might be complicated (see Fig. 1), but they can be captured by some enclosing "repulsive boundaries" discussed in the sequel. Next we define two "paths" around the obstacle $\mathcal{O}_i$, called the *reactive boundary* $\mathcal{R}_i$ and the *repulsive boundary* $\mathcal{Q}_i$ respectively. Similar to the definition of the desired path, one can choose a twice continuously differentiable function $\varphi_i : \mathbb{R}^2 \to \mathbb{R}$ and a nonzero constant c_i such that

$$\mathcal{R}_i = \{\xi \in \mathbb{R}^2 : \varphi_i(\xi) = 0\}, \ \mathcal{Q}_i = \{\xi \in \mathbb{R}^2 : \varphi_i(\xi) = c_i\}, \tag{2}$$

where $c_i \neq 0$. It is assumed that $\mathcal{R}_i$ and $\mathcal{Q}_i$ are one-dimensional compact connected submanifolds in $\mathbb{R}^2$. According to the Jordan curve theorem [19, Section VI.52], $\mathcal{R}_i$ divides the plane $\mathbb{R}^2$ into the bounded open subset $\mathcal{R}_i^{\mathrm{in}}$ (the interior) and the unbounded open subset $\mathcal{R}_i^{\mathrm{ex}}$ (the exterior), and we have $\mathcal{R}_i = \partial \mathcal{R}_i^{\mathrm{in}} = \partial \mathcal{R}_i^{\mathrm{ex}}$, where $\partial(\cdot)$ denotes the

---

[1] Given a positive integer n, the distance between a point $p_0 \in \mathbb{R}^n$ and a nonempty set $\mathcal{S} \subset \mathbb{R}^n$ is denoted by $\mathrm{dist}(p_0, \mathcal{S}) := \inf\{d(p, p_0) : p \in \mathcal{S}\}$, where $d(p, p_0) = \|p - p_0\|_2$ is the Euclidean metric.

boundary of a set. Similarly, the boundary $\mathcal{Q}_i$ divides the plane $\mathbb{R}^2$ into the interior $\mathcal{Q}_i^{\text{in}}$ and the exterior $\mathcal{Q}_i^{\text{ex}}$, and $\mathcal{Q}_i = \partial \mathcal{Q}_i^{\text{in}} = \partial \mathcal{Q}_i^{\text{ex}}$. For convenience, we call $\mathcal{R}_i^{\text{in}}$ the *(open) reactive area*, $\mathcal{R}_i^{\text{ex}}$ the *(open) non-reactive area*, $\mathcal{Q}_i^{\text{in}}$ the *(open) repulsive area* and $\mathcal{Q}_i^{\text{ex}}$ the *(open) non-repulsive area* of the obstacle $\mathcal{O}_i$ respectively. To name the closure of these areas, we simply replace "open" by "closed" (e.g. $\overline{\mathcal{R}_i^{\text{in}}}$ is called the *closed reactive area*, where $\overline{(\cdot)}$ denotes the closure of a set). Intuitively, the reactive area $\mathcal{R}_i^{\text{in}}$ is the area where the robot is near the obstacles and needs to be reactive to obstacles, and the repulsive area $\mathcal{Q}_i^{\text{in}}$ is the area where the robot is forbidden to enter; if the robot's initial position is in $\mathcal{Q}_i^{\text{in}}$, then it is forced to leave (see Fig. 1). Before presenting the following technical assumptions, note that the distance between two non-empty sets $\mathcal{A}$ and $\mathcal{B}$ is denoted by $\text{dist}(\mathcal{A}, \mathcal{B}) := \inf\{\|a - b\|_2 : a \in \mathcal{A}, b \in \mathcal{B}\}$. We further make the following assumptions:

Assumption 2: $\mathcal{O}_i \subset \mathcal{Q}_i^{\text{in}} \subset \mathcal{R}_i^{\text{in}}$ and $\text{dist}(\mathcal{Q}_i, \mathcal{R}_i) > 0$.

Assumption 3: $\mathcal{P} \not\subset \overline{\bigcup_{i \in \mathcal{I}} \mathcal{R}_i^{\text{in}}}$.

Assumption 4: For each $i \neq j \in \mathcal{I}$, $\text{dist}(\mathcal{R}_i^{\text{in}}, \mathcal{R}_j^{\text{in}}) > 0$.

Assumption 2 implies that the reactive and repulsive areas are "induced" by the obstacle inside them, and the repulsive area is naturally "closer to" the obstacle than the reactive area is. Assumption 3 implies that there is at least one segment of the desired path that can be followed by the robot without being "occupied" by the obstacles. Assumption 4 indicates that any two obstacles are sufficiently faraway, and the robot will not enter two different reactive areas at the same time.

C. Problem Definition

In this subsection, we will formally define what a vector-field-based path following problem is when there are obstacles. For the case without obstacles, the definition is found in [20]. First recall that a trajectory $\xi : [0, +\infty) \to \mathbb{R}^n$ asymptotically converges to a non-empty set $\mathcal{A} \subset \mathbb{R}^n$ if for any $\epsilon > 0$, there exists $T > 0$ such that $\text{dist}(\xi(t), \mathcal{A}) < \epsilon$ for $t > T$. In addition, $\dot{\xi}(t)$ denotes $\frac{d}{dt}\xi(t)$ for any function ξ of time t. Now we present the **V**ector **F**ield based integrated **C**ollision **A**voidance and **P**ath **F**ollowing problem (VF-CAPF).

Definition 1: The VF-CAPF problem is to design a continuously differentiable vector field $\chi : \mathbb{R}^2 \to \mathbb{R}^2$ for the differential equation $\dot{\xi}(t) = \chi(\xi(t))$ such that the following four control objectives are satisfied:

1) (Path following). If there are no obstacles ($\mathcal{O}_{\text{all}} = \emptyset$), then the vector field χ enables a robot to follow the desired path [5], [20].

2) (Repulsive $\overline{\mathcal{Q}^{\text{in}}}$). If $\xi(0) \notin \overline{\mathcal{Q}_i^{\text{in}}}$ for all $i \in \mathcal{I}$, then $\xi(t) \notin \overline{\mathcal{Q}_j^{\text{in}}}$ for $t \geq 0$ and all $j \in \mathcal{I}$. If there exits $i \in \mathcal{I}$ such that $\xi(0) \in \overline{\mathcal{Q}_i^{\text{in}}}$, then there exists $T > 0$, such that $\xi(t) \notin \overline{\mathcal{Q}_j^{\text{in}}}$ for $t \geq T$ and all $j \in \mathcal{I}$.

3) (Bounded path error). There exists a positive finite constant M such that $\text{dist}(\xi(t), \mathcal{P}) \leq M$ for $t \geq 0$. Moreover, for all nonempty connected time intervals $\Xi_j \subset \mathbb{R}$, $j \in \mathbb{N}$, such that $\xi(t) \notin \bigcup_i \overline{\mathcal{R}_i^{\text{in}}}$ for $t \in \Xi_j$, the path error $\text{dist}(\xi(t), \mathcal{P})$ is strictly decreasing on Ξ_j.

4) (Penetrable $\overline{\mathcal{R}_i^{\text{in}}}$). Fixing $i \in \mathcal{I}$, if for almost all trajectories, there exists $t_0^e \in \mathbb{R}$ such that $\xi(t_0^e) \in \overline{\mathcal{R}_i^{\text{in}}}$, then there exists $t_0^l > t_0^e$ such that $\xi(t_0^l) \notin \overline{\mathcal{R}_i^{\text{in}}}$. In addition, the trajectory cannot cross the reactive boundary $\mathcal{R}_i$ infinitely fast[2].

Remark 2: In general, to solve the aforementioned vector-field-related problems is mainly about designing an appropriate vector field $\chi : \mathbb{R}^2 \to \mathbb{R}^2$ such that the integral curves of the vector field (that is, the trajectories of the ODE $\dot{\xi}(t) = \chi(\xi)$, where $\xi \in \mathbb{R}^2$) achieve some control objectives. Therefore, after designing the vector field, it is of great importance to investigate the properties of the trajectories, such as the existence and uniqueness of solutions and the convergence results. From the perspective of robotics, the ODE implies that the robot model considered is a simple single-integrator model:

$$\dot{\xi}(t) = u(t), \tag{3}$$

where $\xi(t) = (x(t), y(t))$ represents the position of the robot at time t, and u is the control input that is taken as the designed vector field (i.e., $u(t) = \chi(\xi(t))$). The main motivation behind the simplicity of the model is that the vector field is treated as a guidance signal such that the desired velocity (or orientation) $\chi(\xi)$ is given depending on where the robot is. Then a subsequent robot-model-specific control law could be derived to drive the robot's velocity (or orientation) to approach the desired one. The methodology of first considering the single-integrator robot model and then deriving subsequent control designs for complex robot models, such as the unicycle model, is more general in this sense and has been presented in the literature (e.g., [3], [4], [20]). Due to page limits, the focus of the paper is the design of a composite vector field χ discussed in the following sections, while a robot-model-specific control law will be left as our future work.

III. COMPOSITE VECTOR FIELD VIA BUMP FUNCTIONS

A. Individual Vector Fields

In this subsection, we explain the path following method using a vector field [**?**], [4], [5]. The basic idea is to design a suitable vector field which can guide the robot to move towards and circulate along the desired path. We use the construction of the vector field proposed in [4]. For the desired path in (1) and the reactive boundary in (2), we define the *induced vector field* $\chi_{\mathcal{P}}, \chi_{\mathcal{R}_i} : \mathbb{R}^2 \to \mathbb{R}^2$ associated with $\mathcal{P}$ and $\mathcal{R}_i$ by:

$$\chi_{\mathcal{P}}(\xi) = E\nabla\phi(\xi) - k_p\phi(\xi)\nabla\phi(\xi), \tag{4}$$

$$\chi_{\mathcal{R}_i}(\xi) = E\nabla\varphi_i(\xi) - k_{r_i}\varphi_i(\xi)\nabla\varphi_i(\xi), \tag{5}$$

where $E = \begin{bmatrix} 0 & -1 \\ 1 & 0 \end{bmatrix}$ is the 90° rotation matrix, k_p, k_{r_i} are positive gains and $\nabla(\cdot)$ is the gradient with respect to

---

[2]Suppose there exists a strictly increasing sequence of time instants $(t_i)_{i=1}^{\infty}$ such that a trajectory is in the exit set [21, Definition 2.2] of the reactive boundary at these instants; precisely, $\xi(t_i) \in \mathcal{R}^- := \{\xi_0 \in \mathcal{R} : \xi(0) = \xi_0, \forall \delta > 0, \xi([0, \delta)) \not\subset \mathcal{R}\}$. If $(t_i)_{i=1}^{\infty}$ is a Cauchy sequence, then the trajectory $\xi(t)$ is said to cross $\mathcal{R}$ infinitely fast.

ξ. For convenience, $\chi_{\mathcal{P}}$ is called the *PF (path-following) vector field* and $\chi_{\mathcal{R}_i}$ the *reactive vector field*. The point where a vector field becomes zero is called a *singular point* of the vector field [16, p. 219]. The set of singular points of the vector fields $\chi_{\mathcal{P}}$ and $\chi_{\mathcal{R}_i}$ are denoted by $\mathcal{C}_{\mathcal{P}}$ and $\mathcal{C}_{\mathcal{R}_i}$ respectively. To be more specific,

$$\mathcal{C}_{\mathcal{P}} = \{\xi \in \mathbb{R}^2 : \chi_{\mathcal{P}}(\xi) = 0\} = \{\xi \in \mathbb{R}^2 : \nabla\phi(\xi) = 0\},$$
$$\mathcal{C}_{\mathcal{R}_i} = \{\xi \in \mathbb{R}^2 : \chi_{\mathcal{R}_i}(\xi) = 0\} = \{\xi \in \mathbb{R}^2 : \nabla\varphi_i(\xi) = 0\}.$$

The above equations show that the sets $\mathcal{C}_{\mathcal{P}}$ and $\mathcal{C}_{\mathcal{R}_i}$ are also the sets of *critical points* of ϕ and φ_i respectively. Following [4], we call these sets *critical sets*. Since $\mathcal{P}$, $\mathcal{R}_i$ and $\mathcal{Q}_i$ are one-dimensional connected submanifolds, ϕ has a regular value 0 and φ_i has two regular values 0 and c_i [16, p. 105]. Therefore, we have $\mathcal{P} \cap \mathcal{C}_{\mathcal{P}} = \emptyset$, $\mathcal{R}_i \cap \mathcal{C}_{\mathcal{R}_i} = \emptyset$ and $\mathcal{Q}_i \cap \mathcal{C}_{\mathcal{R}_i} = \emptyset$.

Under some mild assumptions (specifically, Assumptions 1-3 in [4]), which hold for all the examples presented later in this paper, the following lemma regarding convergence results is important [4].

Lemma 1 (dichotomy of convergence): Let $\chi : \mathbb{R}^2 \to \mathbb{R}^2$ be the vector field induced by the one-dimensional connected submanifold (desired path) $\mathcal{P}$ described by (1). Then the trajectory of $\dot{\xi}(t) = \chi(\xi(t))$ converges either to the desired path $\mathcal{P}$ or the critical set $\mathcal{C} := \{\xi \in \mathbb{R}^2 : \chi(\xi) = 0\}$.

Note that the convergence result holds up to a positive scaling of the vector field, as long as the orientation of each vector of χ is not modified [20]. Moreover, the initial conditions where the solution converges to an equilibrium point is characterized by the *stable manifold* defined below.

Definition 2 (stable manifold): Let ξ^* be an equilibrium point of the ordinary differential equation $\dot{\xi}(t) = \chi(\xi(t))$, where $\chi : \mathbb{R}^n \to \mathbb{R}^n$ is a smooth vector field. The stable manifold of ξ^* is the set of all initial values denoted by $\mathcal{W}(\xi^*)$, such that the solution converges to ξ^* if $\xi(0) \in \mathcal{W}(\xi^*)$. In addition, the union of the stable manifold is denoted by $\mathcal{W}(\mathcal{C}) := \bigcup_{\xi^* \in \mathcal{C}} \mathcal{W}(\xi^*)$, where $\mathcal{C} := \{\xi \in \mathbb{R}^n : \chi(\xi) = 0\}$.

B. Bump Functions

The bump functions are inspired by the following lemma originated from "partition of unity" in topology.

Lemma 2 ([16, Proposition 2.25]): Consider an open subset $\mathcal{B} \neq \emptyset$ in $\mathbb{R}^n$ and a closed subset $\mathcal{A} \neq \emptyset$ in $\mathbb{R}^n$ such that $\mathcal{A} \subset \mathcal{B} \subset \mathbb{R}^n$. There exists a smooth function $\sqcap : \mathbb{R}^n \to \mathbb{R}$ such that $\sqcap(x) \equiv 1$ for $x \in \mathcal{A}$, $0 \leq \sqcap(x) \leq 1$ for $x \in \mathcal{B} \setminus \mathcal{A}$ and $\sqcap(x) \equiv 0$ for $x \in \mathbb{R}^n \setminus \mathcal{B}$.

The function $\sqcap$ in Lemma 2 is called a smooth *bump function*, which is a smooth real-valued function that attains 1 on a specified set and attains zero outside a neighborhood of that set [16, p. 42]. Using the same notations in the above lemma, it is easy to conclude that there also exists an "inverted" bump function $\sqcup : \mathbb{R}^n \to \mathbb{R}$ such that $\sqcup(x) \equiv 0$ for $x \in \mathcal{A}$ and $\sqcup(x) \equiv 1$ for $x \in \mathbb{R}^n \setminus \mathcal{B}$ (e.g., letting $\sqcup = 1 - \sqcap$). With abuse of notions, we call $\sqcap$ a *zero-outside bump function* and $\sqcup$ a *zero-inside bump function* intuitively. These functions are useful to "separate" different regions in $\mathbb{R}^n$. In the context of the VF-CAPF problem,
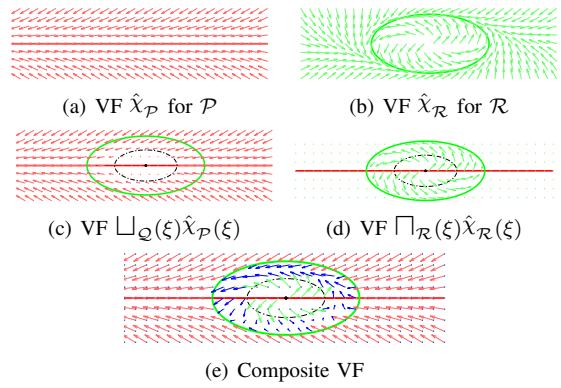

(a) VF $\hat{\chi}_{\mathcal{P}}$ for $\mathcal{P}$ (b) VF $\hat{\chi}_{\mathcal{R}}$ for $\mathcal{R}$

(c) VF $\sqcup_{\mathcal{Q}}(\xi)\hat{\chi}_{\mathcal{P}}(\xi)$ (d) VF $\sqcap_{\mathcal{R}}(\xi)\hat{\chi}_{\mathcal{R}}(\xi)$

(e) Composite VF

Fig. 2. Illustrations of the composite vector field. Given a vector field $\chi : \mathbb{R}^2 \to \mathbb{R}^2$, each arrow in the figure represents a vector $\chi(\xi)$, where $\xi \in \mathbb{R}^2$ is the position of the **tail** rather than the head of the arrow.

these functions can be utilized to integrate different vector fields and reduce the undesirable effects of overlapping. Specifically, the following corollary is given.

Corollary 1: For any reactive boundary $\mathcal{R}_i$ and repulsive boundary $\mathcal{Q}_i$ in (2), $i \in \mathcal{I}$, there exist smooth zero-inside and zero-outside bump functions $\sqcup_{\mathcal{Q}_i}, \sqcap_{\mathcal{R}_i} : \mathbb{R}^2 \to [0, \infty)$ defined below:

$$\sqcup_{\mathcal{Q}_i}(\xi) = \begin{cases} 0 & \xi \in \overline{\mathcal{Q}_i^{\text{in}}} \\ a_i(\xi) & \xi \in \mathcal{Q}_i^{\text{ex}}, \end{cases} \quad \sqcap_{\mathcal{R}_i}(\xi) = \begin{cases} 0 & \xi \in \overline{\mathcal{R}_i^{\text{ex}}} \\ b_i(\xi) & \xi \in \mathcal{R}_i^{\text{in}}, \end{cases} \quad (6)$$

where $a_i : \mathcal{Q}_i^{\text{ex}} \to (0, \infty)$ and $b_i : \mathcal{R}_i^{\text{in}} \to (0, \infty)$ are bounded smooth functions.

C. Composite Vector Field

After introducing the individual vector fields and the bump function above, the composite vector field $\chi_c : \mathcal{D} \subset \mathbb{R}^2 \to \mathbb{R}^2$ is shown as follows:

$$\chi_c(\xi) = \prod_{i \in \mathcal{I}} \sqcup_{\mathcal{Q}_i}(\xi)\hat{\chi}_{\mathcal{P}}(\xi) + \sum_{i \in \mathcal{I}} \sqcap_{\mathcal{R}_i}(\xi)\hat{\chi}_{\mathcal{R}_i}(\xi), \quad (7)$$

where $\hat{(\cdot)}$ is the normalization operator (i.e., for a nonzero vector $v \in \mathbb{R}^n$, $\hat{v} = v/\|v\|$), and $\mathcal{D} = \mathbb{R}^2 \setminus \left(\bigcup_i \mathcal{C}_{\mathcal{R}_i} \bigcup \mathcal{C}_{\mathcal{P}}\right)$ is the domain on which the composite vector field is well-defined. Taking the robot's current position $\xi(t)$ as the feedback signal, the control input in (3) can be taken as $u(t) = \chi_c(\xi(t))$. Therefore, this gives rise to the autonomous ODE: $\dot{\xi}(t) = \chi_c(\xi(t))$, $\xi(0) \in \mathcal{D}$. Since bump functions are smooth and the vector field $\chi_{\mathcal{P}}$ and $\chi_{\mathcal{R}_i}$ are continuously differentiable with respect to ξ, the existence and uniqueness of solutions is guaranteed [22]. For convenience, we define $\mathcal{C}_c := \{\xi \in \mathcal{D} : \chi_c(\xi) = 0\}$, which contains all the equilibria of the differential equation.

IV. MAIN RESULTS

Under Assumption 4 and in view of (7), different reactive vector fields $\chi_{\mathcal{R}_i}$ do not affect one another. Thus, without loss of generality, we only need to consider the case where there is only one obstacle; namely, the index set $\mathcal{I}$ is a singleton. Therefore, all the notations in this section do not have the subscript i. It is also natural to assume that the obstacle is sufficiently close to the desired path such that the robot can perceive the obstacle when on the path (i.e.,

$\mathcal{R}^{\text{in}} \cap \mathcal{P} \neq \emptyset$). Thus, the composite vector field is simplified to

$$\chi_c(\xi) = \begin{cases} b(\xi)\hat{\chi}_{\mathcal{R}}(\xi) & \xi \in \overline{\mathcal{Q}^{\text{in}}} \cap \mathcal{D} \\ a(\xi)\hat{\chi}_{\mathcal{P}}(\xi) + b(\xi)\hat{\chi}_{\mathcal{R}}(\xi) & \xi \in \mathcal{Q}^{\text{ex}} \cap \mathcal{R}^{\text{in}} \cap \mathcal{D} \\ a(\xi)\hat{\chi}_{\mathcal{P}}(\xi) & \xi \in \overline{\mathcal{R}^{\text{ex}}} \cap \mathcal{D}, \end{cases}$$

(8)

where $\mathcal{D} = \mathbb{R}^2 \setminus (\mathcal{C}_{\mathcal{R}} \cup \mathcal{C}_{\mathcal{P}})$. An intuitive illustration is in Fig. 2. If the robot is in $\mathcal{Q}^{\text{in}}$, then only the reactive vector field $\chi_{\mathcal{R}}$ takes effect, while if the robot is in $\overline{\mathcal{R}^{\text{ex}}}$, only the PF vector field $\chi_{\mathcal{P}}$ is effective. However, when the robot is in the *(open) mixed area* $\mathcal{M} := \mathcal{Q}^{\text{ex}} \cap \mathcal{R}^{\text{in}}$, both the PF vector field and the reactive vector field matter. The closure of this area $\overline{\mathcal{M}}$ is called the *closed mixed area*, but note that the vector field is not mixed on the boundaries.

We are now ready to present the main theorem.

Theorem 1: Taking the composite vector field in (7) as the control input to (3), the VF-CAPF problem is solved if the following conditions hold:

1) $\xi(0) \notin \mathcal{W}(\mathcal{C}_{\mathcal{P}})$, $\mathcal{W}(\mathcal{C}_{\mathcal{R}}) \cap \mathcal{Q} = \emptyset$, $\mathcal{C}_{\mathcal{P}}$ is bounded;
2) $\mathcal{C}_{\mathcal{P}} \cap \mathcal{R}^{\text{in}} = \emptyset$ and there is only one equilibrium $c_0 \in \mathcal{C}_c$ in the mixed area $\mathcal{M}$;
3) there exists a trajectory $\xi(t)$ starting from the repulsive boundary $\mathcal{Q}$ and reaching the reactive boundary $\mathcal{R}$.

Proof: Due to page limits, the proof will be given in the full version of the paper. ∎

Remark 3: The conditions in this theorem are rather technical, but in practice, they might be easily satisfied. The stable manifold of the $\mathcal{W}(\mathcal{C}_{\mathcal{R}})$ and $\mathcal{W}(\mathcal{C}_{\mathcal{P}})$ can be numerically computed using the Hadamard's method or the Lyapunov-Perron method [23, Section 3.5]. Fortunately, this process can be omitted for some typical paths, such as circles or ellipses, since they have only one critical point, and the corresponding stable manifold is the critical point itself. Note that it is usually sufficient to model the obstacle as an ellipse; thus, the conditions of this theorem can be greatly simplified. In addition, given a specific desired path $\mathcal{P}$, the important design choices are the repulsive boundary $\mathcal{Q}$, reactive boundary $\mathcal{R}$ and the bump functions. Thus the second condition can be satisfied by changing these design choices. In practice, a better design choice is to narrow down the mixed area $\mathcal{M}$ to reduce the uncertainty of the trajectories. The third condition might be most difficult to verify rigorously, although it itself is not a conservative condition (the existence of only one such trajectory is sufficient). This condition is employed here to eliminate the possibilities of limit cycles in the mixed area, hence ensure that the trajectories are able to leave the mixed area. Note that the proof of existence and non-existence of limit cycles itself is generally a challenging problem in nonlinear system theory, and there are only a few available tools, such as the Poincaré-Bendixson theorem, the Bendixson criterion and the index theory [22, Lemma 2.1-2.3]. These tools might be used to verify the third condition. However, many tested examples satisfy this condition. Intuitively, this can be observed from the plot of the vector field. The vectors in the reactive vector field $\chi_{\mathcal{R}}$ point outward to leave the mixed area, while in
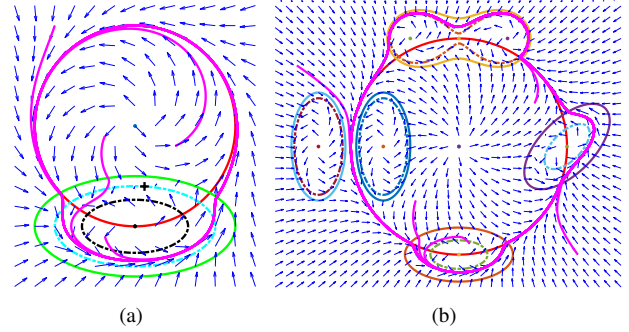

Fig. 3. Simulations. (a) The first simulation; (a) The second simulation.

some regions of the mixed area, the vectors of the PF vector field $\chi_{\mathcal{P}}$ always point from the mixed area to the desired path (e.g., see the vectors in the mixed area in Fig. 3(a)). Therefore, in practice, the third condition might be safely assumed to be true if the repulsive boundary, the reactive boundary and the bump functions are not "pathological". Nevertheless, replacing the third condition by others that are easier to verify in practice is our future work.

V. EXAMPLES

Two examples are illustrated[3]. First, we consider only one obstacle. Specifically, the desired path is a circle described by the implicit function $\phi(x, y) = x^2 + y^2 - R^2 = 0$, where $R > 0$ is the radius. It is shown in [4] that $\mathcal{C}_{\mathcal{P}} = \mathcal{W}(\mathcal{C}_{\mathcal{P}}) = \{(0, 0)\}$. Suppose an obstacle $\mathcal{O}$ is on the path (i.e., $\mathcal{O} \cap \mathcal{P} \neq \emptyset$), and the reactive boundary is described by a rotated ellipse in general: $\varphi(x, y) = ((x - o_x) \cos \beta + (y - o_y) \sin \beta)^2 / a^2 + ((x - o_x) \sin \beta - (y - o_y) \cos \beta)^2 / b^2 - 1 = 0$, where $a, b > 0$ and β is the rotation angle about the center of the ellipse (o_x, o_y). The critical set and the corresponding stable manifold is simply $\mathcal{C}_{\mathcal{R}} = \mathcal{W}(\mathcal{C}_{\mathcal{R}}) = \{(o_x, o_y)\}$. We choose the zero-inside bump function as

$$\sqcup_{\mathcal{Q}}(\xi) = \begin{cases} 0 & \xi \in \{\varphi(\xi) \leq c\} \\ \exp\left(\dfrac{l_1}{c - \varphi(\xi)}\right) & \xi \in \{\varphi(\xi) > c\} \end{cases}$$

(9)

and the zero-outside bump function as

$$\sqcap_{\mathcal{R}}(\xi) = \begin{cases} \exp\left(\dfrac{l_2}{\varphi(\xi)}\right) & \xi \in \{\varphi(\xi) < 0\} \\ 0 & \xi \in \{\varphi(\xi) \geq 0\}, \end{cases}$$

(10)

where $l_1 > 0$, $l_2 > 0$ are used to change the decaying or increasing rate of the bump function. In the first example, we let $R = 1$, $a = 1$, $b = 0.5$, $o_x = 0$, $o_y = -1$, $\beta = 0$, $l_1 = l_2 = 0.1$ and $c = -0.72$. It is easy to verify that the first condition of Theorem 1 is satisfied. It is also verified that $\mathcal{C}_{\mathcal{P}} \cap \mathcal{Q}^{\text{in}} = \emptyset$. To calculate the equilibria in the mixed area, first we note that the equilibria is on the $c/2$-level set of φ (the cyan dashed line in Fig. 3(a)) where the PF vector field and the reactive vector field have the same length. By numerical calculation, there is only one equilibrium point at $(0.094, -0.60)$, which is a saddle point (the black cross in

[3]Supplementary video: https://www.youtube.com/watch?v=C5dmdexs8Oc&feature=youtu.be

Fig. 3(a)). In this case, we assume the third condition of Theorem 1 is true (see Remark 3). The simulation result is shown in Fig. 3(a). The red curve (partly covered by the pink curve) is the desired circular path. The green solid line is the reactive boundary and the black dashed line is the repulsive boundary. The pink curves are the robot trajectories starting from $(0.4, -0.2)$, $(-0.3, -0.1)$, $(-0.8, 1)$ and $(-0.3, -1.1)$ respectively. The figure shows that the robot is able to leave the repulsive area and remain in the non-repulsive area. In addition, when it leaves the reactive area, it follows the desired path successfully.

In the second simulation, we use the same circular desired path and bump functions (with some changes in the parameters), but now there are five obstacles in total, which are modelled by four ellipses and one Cassini oval respectively (see Fig. 3(b)). The repulsive boundaries are shown by dashed lines in the figure. The Cassini oval is described by $\varphi(x, y) = [(x - 0.9)^2 + (y - 2)^2][(x + 0.9)^2 + (y - 2)^2] - 0.9 = 0$. As shown in Fig. 3(b), starting from five different positions: $(-3, 1.5)$, $(-0.8, -1)$, $(1.4, 0.8)$, $(2.2, -2)$ and $(0.2, -1.8)$, all trajectories successfully follow the desired path and bypass the obstacles without entering into the repulsive areas (except starting from the repulsive area). Note that the trajectories smoothly pass the narrow passage surrounded by two "vertical " ellipses, while the artificial potential field method can hardly achieve this [17]. Also note that this method is effective even though there is a concave obstacle, the Cassini oval.

VI. Conclusion and Future Work

We have proposed a general and unified framework to integrate collision avoidance and path following using a composite vector field via bump functions. Rigorous theoretical analysis and numerical simulations have been provided. The desired path and the contours of the obstacles are homeomorphic to a circle or the real line, so no convexity assumptions are required. In addition, since the derivation of the vector field does not involve any specific geometric constraints, the framework is superior in its generality. Moreover, the collision avoidance behaviour is reactive, enabling real-time performances.

Although we have modelled the robot as a point, this does not impair the collision avoidance performance since the repulsive area can be enlarged to take into account the geometric sizes of both the obstacles and the robot. Note that the single-integrator robot model is employed to study the integral curves of the vector field, but it acts as a cornerstone of control law designs for complex robot models without using feedback linearization [4], [20]. However, a valid starting region needs to be identified for a nonholonomic robot so that collision is avoided when the robot is close to obstacles. Also, note that the settings of the paper are essentially different from that of the classic studies [7]; for example, we do not assume that the free space is compact or that the vector field is transverse on the boundary. With regards to moving obstacles, a possible extension is to introduce the time-varying feature of the function φ that characterizes the movement of obstacles. To extend to the three-dimensional case, we will consider the intersection of two surfaces [5].

References

[1] A. P. Aguiar, J. P. Hespanha, and P. V. Kokotović, "Performance limitations in reference tracking and path following for nonlinear systems," *Automatica*, vol. 44, no. 3, pp. 598–610, 2008.

[2] P. B. Sujit, S. Saripalli, and J. B. Sousa, "Unmanned aerial vehicle path following: A survey and analysis of algorithms for fixed-wing unmanned aerial vehicless," *IEEE Control Systems*, vol. 34, no. 1, pp. 42–59, Feb 2014.

[3] V. M. Goncalves, L. C. A. Pimenta, C. A. Maia, B. C. O. Dutra, and G. A. S. Pereira, "Vector fields for robot navigation along time-varying curves in n -dimensions," *IEEE Transactions on Robotics*, vol. 26, no. 4, pp. 647–659, Aug 2010.

[4] Y. A. Kapitanyuk, A. V. Proskurnikov, and M. Cao, "A guiding vector-field algorithm for path-following control of nonholonomic mobile robots," *IEEE Transactions on Control Systems Technology*, vol. PP, no. 99, pp. 1–14, 2017.

[5] W. Yao, Y. A. Kapitanyuk, and M. Cao, "Robotic path following in 3d using a guiding vector field," in *2018 IEEE Conference on Decision and Control (CDC)*. IEEE, 2018, pp. 4475–4480.

[6] O. Khatib, "Real-time obstacle avoidance for manipulators and mobile robots," in *Autonomous robot vehicles*. Springer, 1986, pp. 396–404.

[7] E. Rimon and D. E. Koditschek, "Exact robot navigation using artificial potential functions," *IEEE Transactions on Robotics and Automation*, vol. 8, no. 5, pp. 501–518, Oct 1992.

[8] D. Fox, W. Burgard, and S. Thrun, "The dynamic window approach to collision avoidance," *IEEE Robotics & Automation Magazine*, vol. 4, no. 1, pp. 23–33, 1997.

[9] J. Borenstein and Y. Koren, "The vector field histogram-fast obstacle avoidance for mobile robots," *IEEE transactions on robotics and automation*, vol. 7, no. 3, pp. 278–288, 1991.

[10] M. H. Tanveer, C. T. Recchiuto, and A. Sgorbissa, "Analysis of path following and obstacle avoidance for multiple wheeled robots in a shared workspace," *Robotica*, vol. 37, no. 1, pp. 80–108, 2019.

[11] Y. Zhu, T. Moleski, and J. Wilhelm, "Evaluation of decay functions for vector field based obstacle avoidance," in *AIAA Scitech 2019 Forum*, 2019, p. 1058.

[12] L. Lapierre, R. Zapata, and P. Lepinay, "Combined path-following and obstacle avoidance control of a wheeled robot," *The International Journal of Robotics Research*, vol. 26, no. 4, pp. 361–375, 2007.

[13] A. Sgorbissa and R. Zaccaria, "Integrated obstacle avoidance and path following through a feedback control law," *Journal of Intelligent & Robotic Systems*, vol. 72, no. 3-4, pp. 409–428, 2013.

[14] S. Moe and K. Y. Pettersen, "Set-based line-of-sight (los) path following with collision avoidance for underactuated unmanned surface vessel," in *2016 24th Mediterranean Conference on Control and Automation (MED)*. IEEE, 2016, pp. 402–409.

[15] D. Liberzon, *Switching in systems and control*. Springer Science & Business Media, 2003.

[16] J. Lee, *Introduction to Smooth Manifolds: Second Edition*, ser. Graduate texts in mathematics. Springer, 2015.

[17] Y. Koren and J. Borenstein, "Potential field methods and their inherent limitations for mobile robot navigation," in *Proceedings. 1991 IEEE International Conference on Robotics and Automation*. IEEE, 1991, pp. 1398–1404.

[18] J. Lee, *Introduction to topological manifolds*. Springer Science & Business Media, 2010, vol. 202.

[19] T. Gowers, J. Barrow-Green, and I. Leader, *The Princeton companion to mathematics*. Princeton University Press, 2010.

[20] W. Yao and M. Cao, "Path following control in 3d for nonholonomic robots using a vector field," 2019, under review.

[21] C. C. Conley, *Isolated invariant sets and the Morse index*. American Mathematical Soc., 1978, no. 38.

[22] H. Khalil, *Nonlinear Systems*, 3rd ed. Prentice Hall, 2002.

[23] S. Wiggins, *Introduction to applied nonlinear dynamical systems and chaos*. Springer Science & Business Media, 2003, vol. 2.